ADVANCED ENERGY MATERIALS
www.advenergymat.de

Multi-Selenophene Strategy Enables Dimeric Acceptors-Based Organic Solar Cells with over 18.5% Efficiency

Yuyang Bai, Tianqi Chen, Xinyi Ji, Jiaying Wang, Wenkai Zhao, Shaohui Yuan, Yunxin Zhang, Guankui Long, Zhe Zhang, Xiangjian Wan, Bin Kan,* and Yongsheng Chen*

Dimeric acceptor (DMA) becomes a promising alternative to small-molecular and polymeric acceptor-based organic solar cells (OSCs) due to its well-defined chemical structure, high batch-to-batch reproducibility, and low molecular diffusion properties. However, DMAs usually exhibit blueshifted absorptions, limiting their photon utilization abilities. Herein, multi-selenophene strategies are adopted to develop redshifted DMAs. From monomer (YSe) to dimers (DYSe-1 and DYSe-2), reduced electron reorganization energies and exciton binding energies enable the efficient charge dynamics in the DMAs-based OSCs. Together with their effective absorption extending to ≈920 nm, DYSe-1- and DYSe-2-based OSCs exhibit outstanding short-circuit current densities (J_{SC}s) over 27 mA cm^{-2}, which are the best among DMAs. Besides, compared with the YSe-based device, both DMA-based devices have higher electroluminescence quantum efficiencies and thus reduce nonradiative recombination loss (ΔE_3), contributing to their reduced energy losses. The resultant open-circuit voltages (V_{OC}s) of DYSe-1- and DYSe-2- based OSCs are ≈0.88 V, which, combining their super J_{SC} values, lead to the promising power conversion efficiencies of 18.56% and 18.22%, respectively. These results are among the best in DMAs-based OSCs and highlight the great potential of the multi-selenophene strategy for the development of redshifted DMAs with high performance.

1. Introduction

Solution-processable organic solar cells (OSCs) have garnered much attention due to their advantages of lightweight, flexible, and large-area manufacturing.[1] In OSCs, organic photovoltaic materials with diverse chemical structures play a decisive role in improving power conversion efficiency (PCE) and device stability.[2] In particular, small-molecule acceptors (SMAs) with acceptor–donor–acceptor (A–D–A) structures offer a way to solve the trade-off between open-circuit voltage (V_{OC}) and short-circuit current density (J_{SC}) in fullerene acceptor–based OSCs, thereby boosting NFA-based OSCs.[3] As suitable alternatives to $PC_{71}BM$, ITIC and its analogs offer the advantages of a planar A–D–A backbone, satisfactory electron mobility, and an effective absorption range extending to ≈850 nm, consequently achieving maximum PCEs of >15% when blended with wide-bandgap polymer donors.[4] The emergence of Y6 and its analogs, with absorption ranges redshifted to >950 nm, has improved the state-of-the-art OSCs, with super PCEs exceeding 19% recently.[5] Especially, broad photoelectrical conversion ranges observed for Y acceptor-based blend films offer a platform for achieving outstanding J_{SC} values (26–28 mA cm^{-2}), which is a factor in their much-improved PCEs.[6] According to the semiempirical prediction results, near-infrared acceptor materials with effective absorption in the range of 880–930 nm have great potential to realize single-layer OSCs with PCEs exceeding 20%.[7]

Despite the progress in the PCEs of SMA-based OSCs, these devices still suffer from challenges such as undesired stability and energy losses (E_{loss}).[8] Recently, some creative strategies have been proposed to improve the thermodynamic stability of bulk heterojunction layers, such as introducing materials with high glass transition temperature (T_g) into the active layer or fabricating all-polymer active layers.[9] Among them, dimeric acceptors (DMAs) are popular for molecular construction as they inherit the advantages of SMAs and polymeric SMAs (PSMAs). Furthermore, they exhibit characteristics such as well-defined chemical structure, high batch-to-batch reproducibility, and low molecular diffusion, thereby realizing binary devices with high PCEs over >18%.[10] More importantly, compared with

Y. Bai, T. Chen, X. Ji, J. Wang, W. Zhao, S. Yuan, Y. Zhang, G. Long, B. Kan
School of Materials Science and Engineering
National Institute for Advanced Materials
Nankai University
Tianjin 300350, China
E-mail: xyji06@nankai.edu.cn; kanbin04@nankai.edu.cn
Z. Zhang, X. Wan, Y. Chen
State Key Laboratory and Institute of Elemento-Organic Chemistry
Frontiers Science Center for New Organic Matter
The Centre of Nanoscale Science and Technology and Key Laboratory of Functional Polymer Materials
Renewable Energy Conversion and Storage Center (RECAST)
College of Chemistry
Nankai University
Tianjin 300071, China

The ORCID identification number(s) for the author(s) of this article can be found under https://doi.org/10.1002/aenm.202400938

DOI: 10.1002/aenm.202400938

SMA- and PSMA-based OSCs, DMA-based devices display reduced E_{loss} and improved device stability simultaneously, showing broad prospects for the development of high-performance OSCs.[11] However, compared with typical SMAs, π-bridge-linked DMAs usually have less coplanar conjugated backbones and therefore exhibit blueshifted absorption in the solid state, limiting their photon utilization abilities to some extent. Hence, the J_{SC} values of DMA-based devices are inferior to those of SMA-based devices, hindering the development of high-performance DMA-based OSCs.[12]

The design and construction strategies of DMAs with redshifted absorption (referred to as redshifted DMAs for brevity) remain underexplored. Considering that the basic properties of DMAs largely depend on those of the corresponding SMAs, redshifted DMAs can be developed based on SMAs with strong near-infrared absorptions. Among various strategies, the replacement of thiophene with selenophene is one of the most effective and widely adopted strategies for expanding the redshifted absorption range of SMAs.[13] The increased electron-cloud delocalization of selenium (compared with that of sulfur) usually results in relatively large orbital overlap in π-conjugated systems and thus enhanced quinone properties, which contributed to the extended redshifted absorption in such SMAs without considerable changes in their molecular structure and geometry.[14] Based on Y6 structures, numerous selenium-substituted SMAs have been successfully developed to realize outstanding J_{SC} (>28 mA cm^{-2}), showing great potential for OSC fabrication. However, the optimal PCE for most selenophene-based SMAs remains less than 19% because of the relatively low V_{OC} values and fill factors (FFs).[15] The advantages of the selenium substitution strategy and DMAs can be maximized by exploring multiselenium-substituted DMAs to develop redshifted DMAs with reduced E_{loss} and high PCEs. However, a feasible strategy for synthesizing such a DMA remains unreported to date.

Herein, based on the YSe monomer, we used multi-selenophene substitution to prepare two selenium-substituted DMAs: DYSe-1 and DYSe-2. The linkers between the two wings of DYSe-1 (thiophene) and DYSe-2 (selenophene) were shown to have little impact on their properties. Compared with YSe, DYSe-1, and DYSe-2 not only inherited effective redshifted absorption profiles but also displayed reduced electron reorganization energies and lower exciton binding energies. The reduced molecular self-aggregation in the dimer-based blend (PM6:DYSe-1 and PM6:DYSe-2) films compared with that in the monomer-based blend film resulted in more suitable and consistent D/A phase separation. Hence, the DMA-based blends exhibited optimized charge dynamics properties, and DYSe-1- and DYSe-2-based OSCs achieved remarkable J_{SC} values of >27 mA cm^{-2}, thus ranking the best among DMA-based binary devices. Furthermore, they exhibited reduced E_{loss} values, reasonably high V_{OC} values (≈0.88 V), and excellent PCEs (>18%). Notably, a high PCE of 18.56% is realized in PM6:DYSe-1-based OSC. Thus, our work is the first-time report of multiselenophene-substituted DMA-based OSCs with PCEs of >18% and highlights the great potential of the multi-selenophene strategy for the development of high-performance DMAs.

2. Results and Discussion

2.1. Materials Design and Properties

The chemical structures and syntheses of the small-molecule YSe and dimeric DYSe-1/DYSe-2 are presented in **Figure 1a** and Scheme S1 (Supporting Information), respectively. The selenium-substituted fused-ring unit, namely 12,13-bis(2-hexyldecyl)−3,9-diundecyl-12,13-dihydroselenopheno[2″,3″:4′,5′]thieno[2′,3′:4,5]pyrrolo[3,2-g]selenopheno[2′,3′:4,5]thieno[3,2-b][1,2,5]thiadiazolo[3,4-e]indole (**1**), was prepared in satisfactory yields as described elsewhere.[13] The subsequent Vilsmeier–Haack reaction produced monoaldehyde-substituted **2-1** and dialdehyde-substituted **2-2** in yields of 85% and 10%, respectively. The Knoevenagel condensation reaction between **2-1** and 2-(5-bromo-3-oxo-2,3-dihydro-1H-inden-1-ylidene)malononitrile (Br-IC) produced **3**, which was further functionalized with a monoaldehyde unit to obtain **4**. In turn, **4** was converted into the desired dimeric molecules in two steps involving the Stille coupling and Knoevenagel condensation. In addition, YSe was prepared as a reference in high yield.

Molecular surface electrostatic potentials (ESPs) were calculated to understand the difference in electronic structures between the monomer (YSe) and dimers (DYSe-1/DYSe-2). Most molecular surfaces exhibited positive ESPs, indicating their electron-accepting nature (Figure 1b).[14] The average ESP of DYSe-1/DYSe-2 was slightly lower than that of YSe (Figure S1, Supporting Information), and a more uniform distribution of ESP facilitated charge transport within dimeric molecules. In addition, with the introduction of bridging units in DYSe-1/DYSe-2, their molecular structures obtained a continuous A–D–A structure, which was more conducive to intramolecular charge transport. Additionally, this resulted in larger dipole moments for DYSe-1 (2.84 Debye) and DYSe-2 (2.12 Debye) than YSe (1.67 Debye), facilitating molecular aggregation by promoting intermolecular interactions and stacking.[16]

To study the optical properties of three acceptors, the UV–vis absorption spectra of YSe, DYSe-1, and DYSe-2 were measured in chloroform solutions (Figure S2, Supporting Information) and film states (**Figure 2a**). In diluted solutions, all of them exhibited strong absorption in the range of 450–800 nm, and the absorption peaks (λ_{sol}) of YSe, DYSe-1, and DYSe-2 were located at 740, 748, and 748 nm (**Table 1**; Figure S2, Supporting Information), respectively. The corresponding molar extinction coefficients increased in the order of YSe (1.10×10^5 M^{-1} cm^{-1}) < DYSe-1 (1.89×10^5 M^{-1} cm^{-1}) < DYSe-2 (1.99×10^5 M^{-1} cm^{-1}), which was attributed to the increased conjugation length and strengthened ICT effect of DYSe-1/DYSe-2 by the introduction of election-rich selenophene in dimeric acceptors. Compared with their absorption in diluted solution, the absorption spectra of YSe-, DYSe-1-, and DYSe-2-based thin films exhibited wider redshifted absorption peaks, extending to the near-infrared range (Figure 2a). In addition, the maximum absorption peaks for YSe-, DYSe-1-, and DYSe-2-based films were observed at 836, 820, and 822 nm, respectively, corresponding to redshifts of 96, 72, and 74 nm, respectively, compared with their solutions. The different redshifted characters of the monomer and dimers were

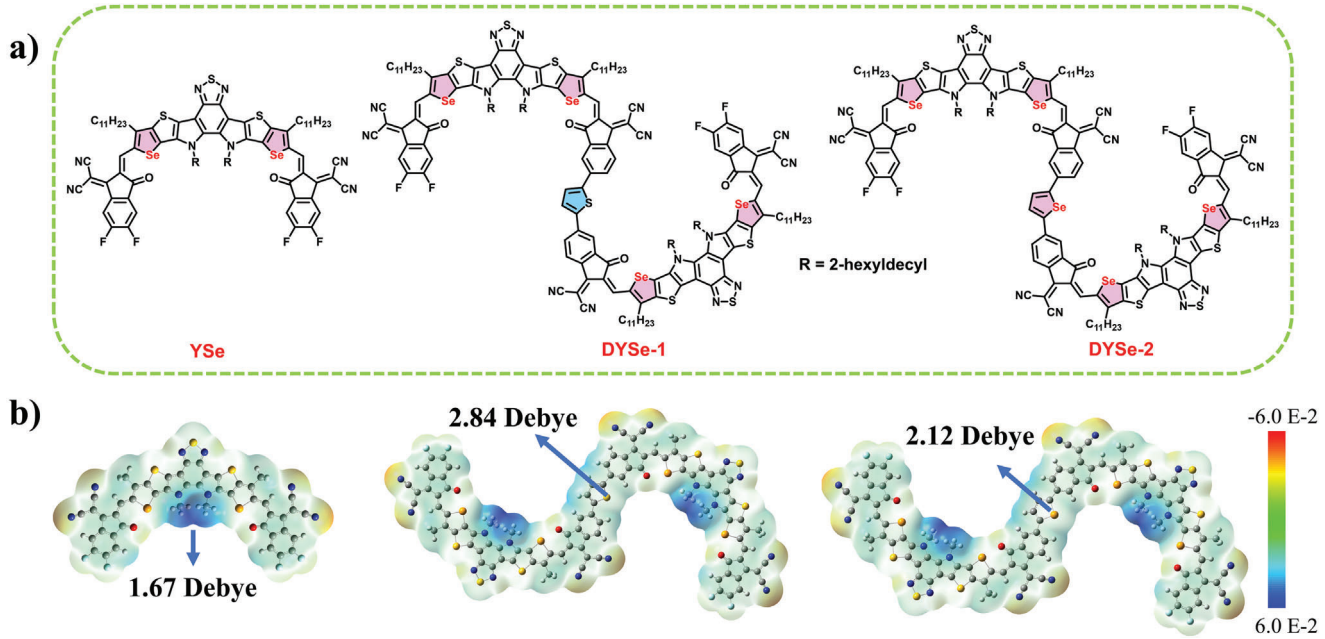

Figure 1. a) The chemical structures of YSe, DYSe-1, and DYSe-2, respectively. b) Electrostatic surface potential (ESP) distributions and dipole moments of YSe, DYSe-1 and DYSe-2, respectively.

associated with their molecular packing properties, as revealed by the subsequent grazing-incidence wide-angle X-ray scattering (GIWAXS) measurements.

The energy levels of the three molecules and PM6 polymer in the solid state were estimated via cyclic voltammetry under identical conditions to study the energy offsets between electron donors and acceptors (Figure S3, Supporting Information). According to the energy diagrams shown in Figure 2b, the highest occupied molecular orbital (HOMO) and lowest unoccupied molecular orbital (LUMO) of YSe were located at −5.71 and −3.85 eV, respectively. Once the two YSe wings were combined to form DYSe-1 and DYSe-2, the HOMO (−5.67 and −5.68 eV, respectively) and LUMO (−3.82 and −3.83 eV, respectively) shifted to higher energies, in line with the results of density functional theory calculations (Figure S4, Supporting Information). Notably, different linkers in the two DMAs negligibly affected their energy levels. The slightly higher (compared with that of YSe) LUMO energies of the dimers helped in achieving a better V_{OC} upon blending with PM6 as a polymer donor. In addition, differences among the LUMO and HOMO energies of PM6 and DYSe-1/DYSe-2 were within the range of 0.15–0.24 eV, i.e., large enough to drive exciton dissociations in the corresponding blend films.[17]

The electron reorganization energies (λ_e) of YSe, DYSe-1, and DYSe-2 were calculated as 176, 83.3, and 83.1 meV, respectively, (Figure 2c) according to previously reported methods.[18] Low λ_e, which has also been observed in acceptors other than DYSe-1 and DYSe-2, is thought to favor electron transportation.[19] Exciton kinetics in YSe, DYSe-1, and DYSe-2 neat films were probed by temperature-dependent steady photoluminescence spectroscopy (Figure 2d).[20] The exciton binding energy (E_b) was determined by solving the equation $I(T) = I_0/[1 + A\exp(-E_b/k_BT)]$ and decreased in the order of YSe (≈317 meV) > DYSe-2 (230 meV) > DYSe-1 (220 meV) (Figure S5, Supporting Information). Therefore, despite the decreased HOMO energy offsets between PM6 and the dimers, the corresponding devices were expected to exhibit high exciton dissociation and charge generation efficiencies.

The molecular packing motifs in the three neat films were probed by GIWAXS measurements, with the corresponding diffraction patterns shown in Figure 2e and line-cut profiles in in-plane (IP) and out-of-plane (OOP) directions shown in Figure S6 (Supporting Information). The (010) peak in the OOP direction and (100) peak in the IP direction were observed in all cases, indicating that YSe, DYSe-1, and DYSe-2 preferentially adopted face-on molecular orientations. For the YSe neat film, the above peaks were located at 1.64 and 0.30 Å, respectively, which gives a

Table 1. Optical properties and energy levels of YSe, DYSe-1, and DYSe-2.

	$\lambda_{max}^{sol.}$ [nm]	ε_{max} [×10^5 M^{-1} cm^{-1}]	λ_{max}^{film} [nm]	$\Delta\lambda^{s\text{-}f}$ [nm]	E_{LUMO} [a)] [eV]	E_{HOMO} [a)] [eV]	E_{LUMO} [b)] [eV]	E_{HOMO} [b)] [eV]
YSe	740	1.10	836	96	−3.85	−5.71	−3.85	−5.83
DYSe-1	748	1.89	820	72	−3.82	−5.67	−3.87	−5.77
DYSe-2	748	1.99	822	74	−3.83	−5.68	−3.87	−5.78

[a)] Energy Level was calculated by CV; [b)] Energy Level calculated by DFT.

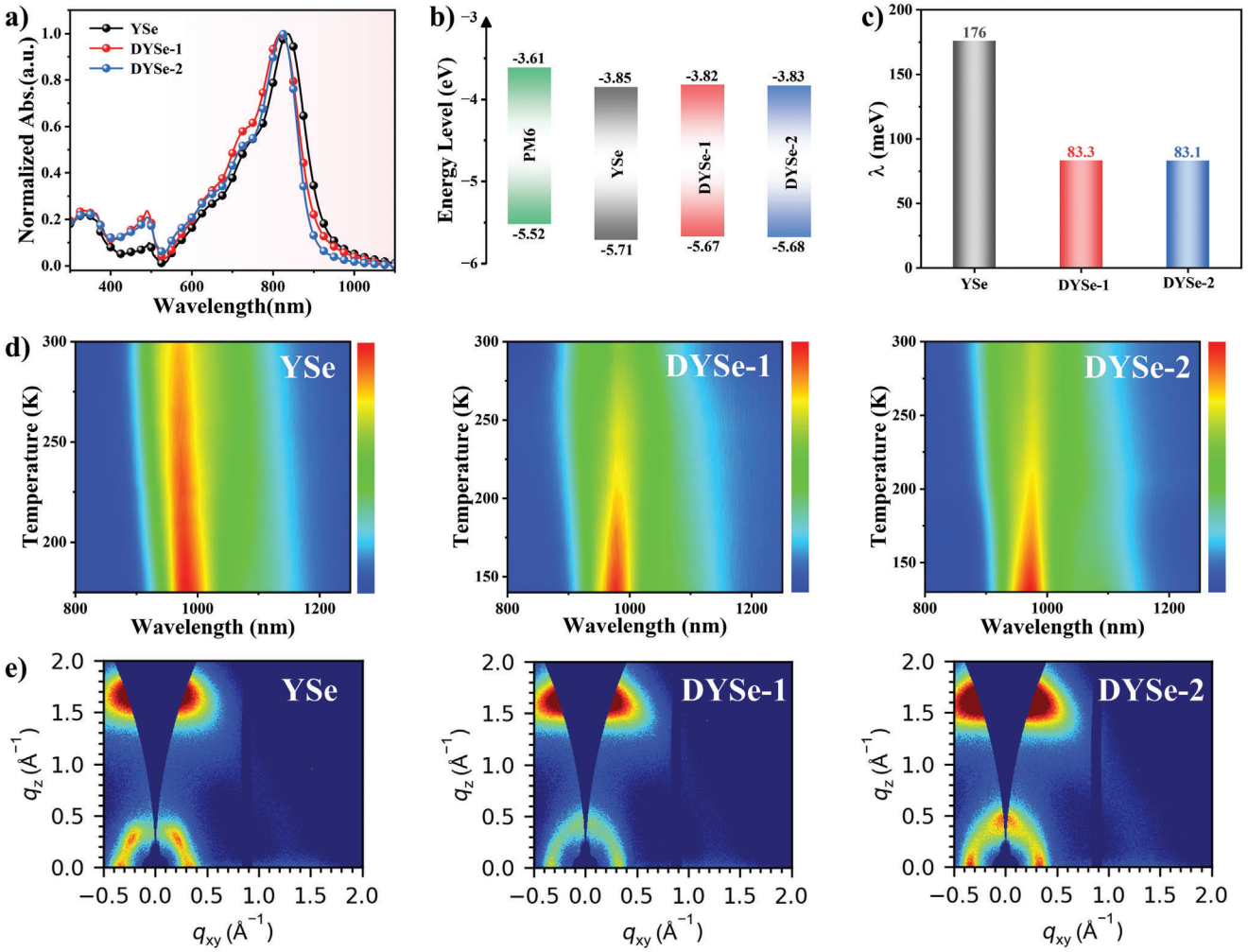

Figure 2. a) Normalized absorption profiles of YSe, DYSe-1 and DYSe-2. b) The Energy levels of PM6, YSe, DYSe-1 and DYSe-2. c) The electron reorganization energy of YSe, DYSe-1, and DYSe-2. d) The temperature-dependent PL spectra of YSe, DYSe-1, and DYSe-2 neat films, respectively. e) GIWAXS images of YSe-, DYSe-1-, and DYSe-2-based neat films, respectively.

π–π stacking distance ($d_{\pi-\pi}$) of 3.83 Å and an alkyl-to-alkyl stacking distance of 20.94 Å. When the two monomers were linked by bridging units to form dimers, the π–π stacking distance increased to 3.93 Å for DYSe-1 and 4.00 Å for DYSe-2 (Table S1, Supporting Information). The coherence lengths (CLs) of the (010) peak in the OOP direction and the (100) peak in the IP direction for DYSe-1/2 exceeded that for YSe (Figure S7 and Table S1, Supporting Information), alleviating the adverse effect of the increased π–π stacking distance in the dimers on charge transport. In addition, the replacement of the thiophene linker in DYSe-1 with the selenophene linker in DYSe-1 increased $d_{\pi-\pi}$ and reduced the CL, which highlighted the various effects of the selenophene unit on different positions in the molecular backbones.

2.2. Photovoltaic Properties

The photovoltaic performances of YSe, DYSe-1, and DYSe-2 were explored using conventional devices configured as ITO/2Br-2PACz/active layer/PNDIT-F3N/Ag and prepared as described in Supporting Information. The wide-bandgap PM6 polymer was used as an electron donor, and the effects of the D:A ratio and other parameters on cell performance were examined (Table S2–S4, Supporting Information). The optimal current density–voltage (J–V) curves are shown in **Figure 3**a, and the corresponding photovoltaic parameters are summarized in **Table 2**. The PM6:YSe-based device yielded an exceptional J_{SC} of 28.03 mA cm^{-2}, partially attributable to its broad and efficient absorption. The slightly low V_{OC} of ≈0.820 V limited the overall PCE of the above device to 17.08%, which was consistent with the values reported for YSe analog-based OSCs.[14–21] Furthermore, similar to YSe, DYSe-1- and DYSe-2-based devices maintained excellent J_{SC} values of >27 mA cm^{-2}, indicating the success of the multiselenophene-based DMA construction strategy. Notably, the J_{SC} of the DYSe-1-based device (27.51 mA cm^{-2}) exceeded those previously reported for DMA-based OSCs and most SMA-based devices.[22] More importantly, the remarkably improved V_{OC} of ≈0.880 V together with slightly increased *FF*s contributed to the large

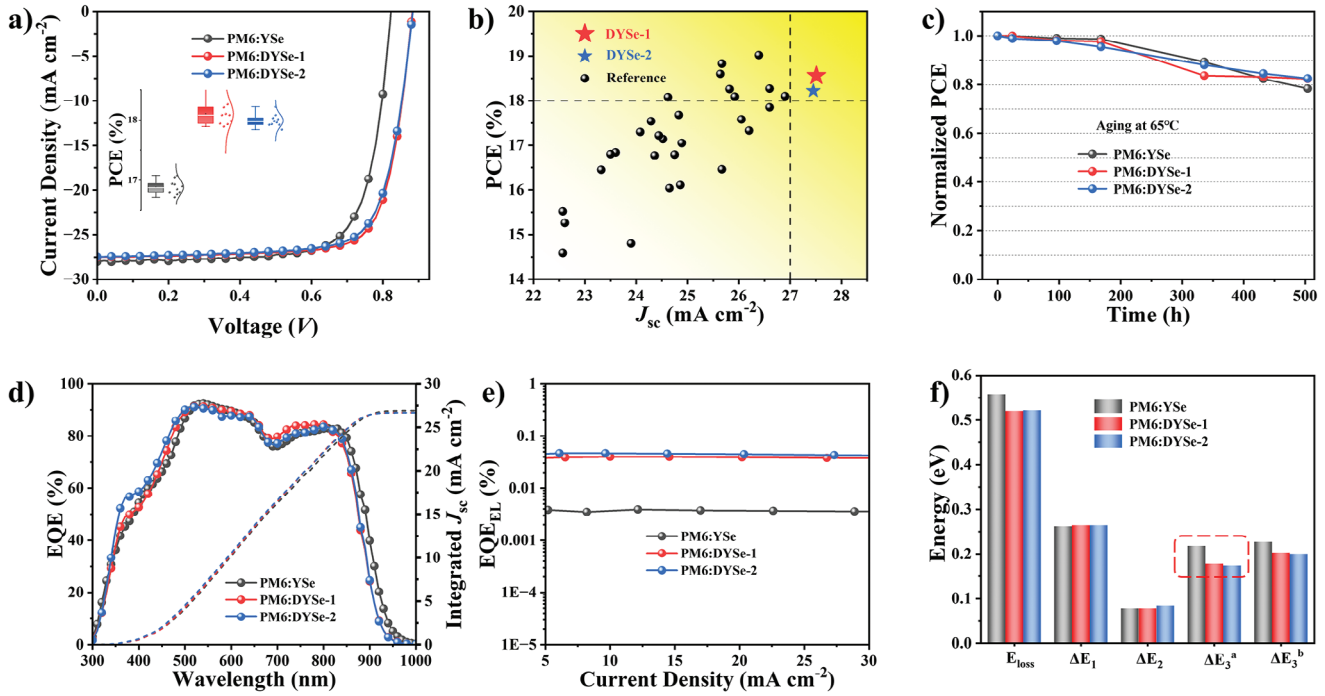

Figure 3. a) *J–V* curves of PM6: YSe/DYSe-1/DYSe-2 based optimized devices, and the inserted Figure shows the distribution of 10 devices. b) A summary of the Jsc and PCE of binary OSCs based on dimeric acceptors. c) Thermal stability of three blends-based optimal devices. d) EQE curves and integrated Jsc curves of PM6: YSe/DYSe-1/DYSe-2 based devices, respectively. e) EQE_{EL} curves of PM6: YSe/DYSe-1/DYSe-2 based devices. f) Energy losses of PM6: YSe/DYSe-1/DYSe-2, and ΔE_3^a is calculated from qV_{rad}^{oc}-qV^{oc}, ΔE_3^b is calculated from -kTln(EQE_{EL}).

(>18%) PCEs of PM6:DYSe-1- and PM6:DYSe-2-based devices. To the best of our knowledge, this is the first study where the multiselenophene substitution strategy was successfully applied to the construction of high-performance DMA-based OSCs with PCEs of >18%. As summarized in Table S5 (Supporting Information) and depicted in Figure 3b, both two DMA-based devices are the rare successful cases with high J_{SC}s (>27 mA cm^{-2}) and PCEs (>18%) simultaneously. The small difference between the PCEs of DYSe-1- and DYSe-2-based devices (18.56% and 18.22%, respectively) was ascribed to fluctuations in their parameters (V_{OC}/J_{SC}/FF) caused by their slightly different charge dynamics, as discussed below. The thermal stability of all fabricated devices was investigated by heating at 65 °C in a nitrogen-filled glovebox. The DYSe-1- and DYSe-2-based devices maintained >80% of their original PCEs after thermal aging for >500 h (Figure 3c), thus having acceptable T_{80} lifetimes.

Figure 3d presents the external quantum efficiency (EQE) spectra of the optimal devices and their integrated J_{SC} curves. The observed absorption trend accounted for varied photoelectron response ranges, with the PM6:YSe-based device exhibiting broader and more redshifted EQE responses than the PM6:DYSe-1- and PM6:DYSe-2-based devices. In the 300–830 nm range, the integrated J_{SC}^{cal} values reached 23.35, 23.79, and 23.73 mA cm^{-2} for YSe-, DYSe-1-, and DYSe-2-based devices, respectively. For the YSe-based device, the J_{SC}^{cal} value in the range of >830 nm equaled 3.57 mA cm^{-2}, exceeding the values of the DYSe-1/DYSe-2-based devices by ≈0.70 mA cm^{-2}. These results implied that the higher J_{SC} of the YSe-based device mainly originates from its redshifted photoelectron response range. In general, the total J_{SC}^{cal} for all devices (Table 2) corresponded well (≈4% mismatch) with those extracted from the *J–V* curves, supporting the reliability of our results.

As mentioned earlier, different V_{OC} values played an important role in determining PCEs; hence, a detailed E_{loss} analysis was conducted according to the detailed balance theory (Figures S8 and S9 , Supporting Information). The optical band gaps (E_g) of the PM6:YSe, PM6:DYSe-1, and PM6:DYSe-2 blend films were obtained from the derivatives of the corresponding EQE curves as 1.381, 1.405, and 1.406 eV, respectively. The E_{loss} (estimated as $E_{loss} = E_g - qV_{oc}$) of the PM6:YSe-based device (0.558 eV)

Table 2. Photovoltaic performance parameters of best devices based on YSe, DYSe-1, and DYSe-2, respectively.

BHJ	V_{oc} [V]	J_{sc} [mA cm^{-2}]	$J_{sc,cal}$ [mA cm^{-2}]	FF [%]	PCE [%]
PM6:YSe	0.823 (0.820 ± 0.003)	28.03 (27.97 ± 0.06)	26.93	74.2 (73.9 ± 0.4)	17.08 (16.88 ± 0.20)
PM6:DYSe-1	0.885 (0.881 ± 0.004)	27.51 (27.47 ± 0.04)	26.69	76.6 (76.4 ± 0.3)	18.56 (18.43 ± 0.12)
PM6:DYSe-2	0.884 (0.881 ± 0.003)	27.45 (27.38 ± 0.05)	26.68	75.2 (74.8 ± 0.4)	18.22 (18.11 ± 0.13)

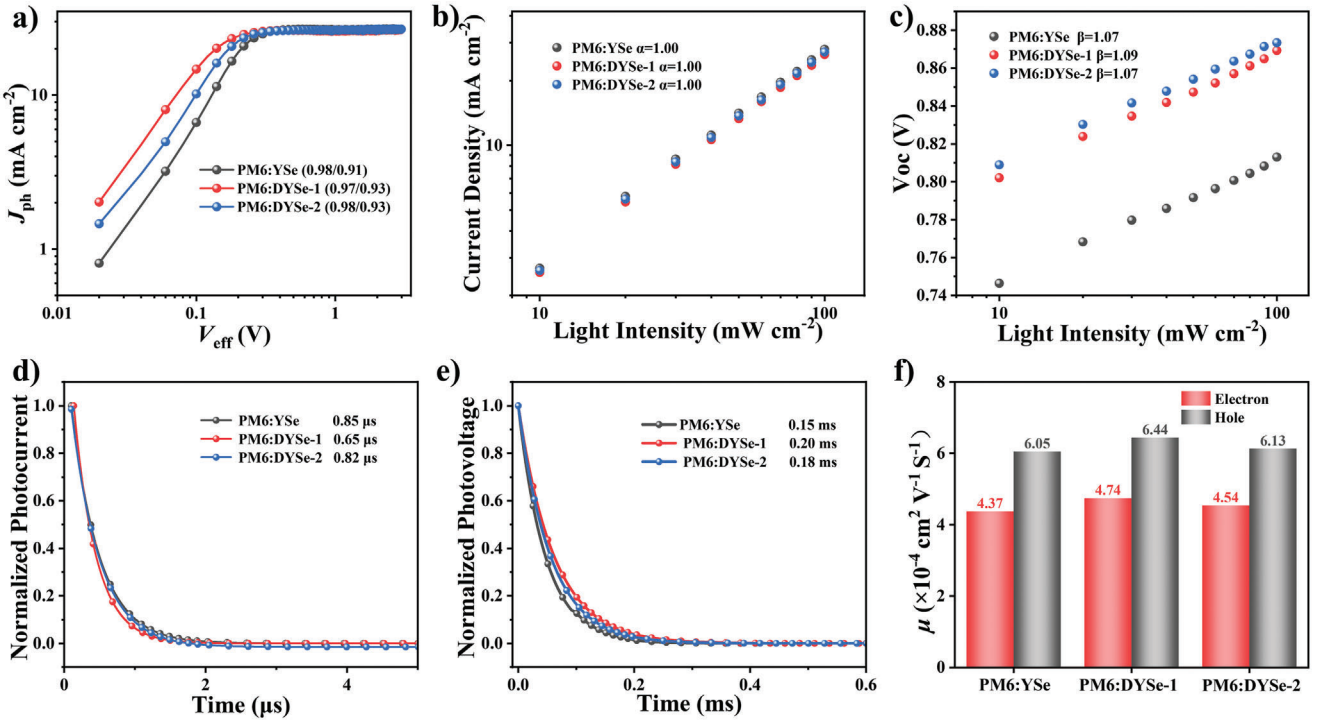

Figure 4. a) J_{ph}-V_{eff} versus. b) Current density (Jsc) versus Light Intensity. c) Voc versus Light Intensity. d) Transient photocurrent (TPC) and e) Transient photovoltage (TPV) measurements of devices based on PM6: YSe/DYSe-1/DYSe-2. f) Histograms of the electron mobility (μ_e) and hole mobility (μ_h).

was ≈0.03 eV higher than those of PM6:DYSe-1- (0.520 eV) and PM6:DYSe-2-based (0.522 eV) devices. The three optimized devices had almost identical radiative recombination energy losses above the band gap (ΔE_1) and similar radiative recombination losses below the bandgap (ΔE_2) (Table S6, Supporting Information). Thus, nonradiative recombination (ΔE_3) was the main factor responsible for the decrease in E_{loss} upon going from YSe- to DYSe-1/DYSe-2-based devices. Compared with the YSe-based device, both DMA-based devices had similar higher electroluminescence quantum efficiencies (EQE_{EL}) and thus lower ΔE_3 (Figure 3e,f), which explained the reduced E_{loss} of the latter devices.

2.3. Charge Dynamic Properties

The relationship between photocurrent density (J_{ph}) and effective voltage (V_{eff}) was investigated to clarify the charge generation and recombination behaviors of the fabricated devices. YSe-, DYSe-1-, and DYSe-2-based devices had exciton dissociation efficiencies exceeding 0.97 (**Figure** 4a), which indicated efficient charge generation, while the respective charge collection efficiencies equaled 0.91, 0.93, and 0.93. The increase in the charge collection efficiency upon going from YSe to DYSe-1 and DYSe-2 was attributed to the more favorable molecular packing in the latter blends and the optimized morphologies of the corresponding films, as discussed in detail below. Furthermore, the J_{SC}–light intensity (P) plots suggested that the relationship between these parameters can be defined as $J_{SC} \propto P^S$ (Figure 4b).[23] The three optimal devices showed similar close-to-unity S-values indicative of negligible bimolecular recombination. In addition, the slope of V_{OC}–P was explored to analyze the trap-assisted recombination mechanism. If the slope was close to 1 kT q^{-1}, bimolecular recombination was the dominant recombination mechanism. Conversely, a slope value approaching 2 kT q^{-1} indicated that trap-assisted recombination is the main recombination loss channel. As shown in Figure 4c, the V_{OC}–P curves of PM6:YSe/DYSe-1/DYSe-2–based devices had slopes of 1.07, 1.09, and 1.07, respectively, which suggested rather similar suppressed trap-assisted recombination in all blends.

Transient photocurrent (TPC) and transient photovoltage (TPV) measurements were further conducted to study the charge dynamic properties of the OSCs. The charge extraction time decreased in the order of PM6:DYSe-1 (0.65 μs)<PM6:DYSe-2 (0.82 μs)<PM6:YSe (0.85 μs) (Figure 4d), which implied that less charge was trapped in the DMA-based devices. Additionally, the photogenerated carrier lifetime of PM6:YSe derived from its TPV profile (0.15 ms) was considerably shorter than those of PM6:DYSe-1 (0.20 ms) and PM6:DYSe-2 (0.18 ms), indicating suppressed charge carrier recombination in the DMA-based devices (Figure 4e). Note that the DYSe-1-based device exhibited the best charge dynamic behavior, as supported by its shortest charge extension time (0.65 μs) and longest carrier lifetime (0.20 ms). Given that these values are directly related to charge mobility, the space-charge-limited current method was used to measure hole (μ_h) and electron (μ_e) mobilities in the blend films. The μ_e and μ_h of PM6:YSe-based device were 4.37 × 10^{-4} and 6.05 × 10^{-4} cm^2 V^{-1} s^{-1}. When YSe linked with bridging units, μ_e and μ_h improved to 4.74 × 10^{-4} and 6.44 × 10^{-4} cm^2 V^{-1} s^{-1} for DYSe-1 and 6.13 × 10^{-4} and 4.54 × 10^{-4} cm^2 V^{-1} s^{-1} for

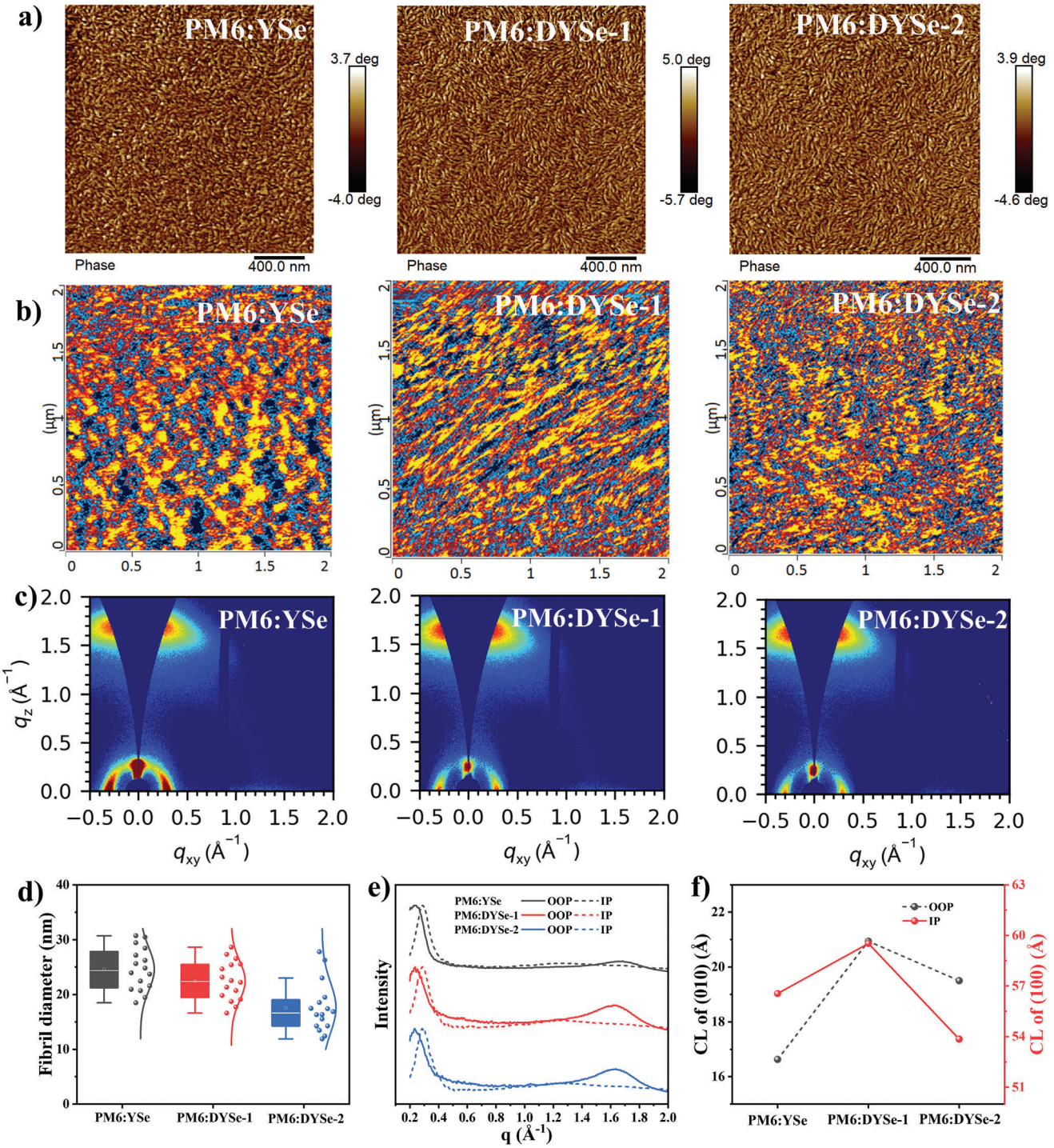

Figure 5. a) AFM phase images, b) AFM-IR images, and c) GIWAXS images of PM6:YSe/DYSe-1/DYSe-2 blend films, respectively. d) The distribution of the fibril width for PM6: YSe/DYSe-1/DYSe-2 blend films. e) Line-cut profiles in in-plane (IP) and out-of-plane (OOP) of GIWAXS. f) Coherence length of (010) and d-packing in OOP for PM6:YSe/DYSe-1/DYSe-2 films.

DYSe-2, respectively (Figure 4f; Figure S10, Supporting Information). Compared with the PM6:DYSe-2-based device, the PM6:DYSe-1-based device exhibited higher and more balanced mobility, which explains its best FF to some extent. Besides, the μ_e of YSe neat film was measured to be 4.68×10^{-4} cm^2 V^{-1} s^{-1}, which was enhanced to be 5.31×10^{-4} cm^2 V^{-1} s^{-1} for DYSe-1 neat film and 5.04×10^{-4} cm^2 V^{-1} s^{-1} for DYSe-2 neat film, respectively (Figures S11 and S12, Supporting Information). Thus, the DMA-based devices exhibited efficient charge generation and reduced charge recombination dynamics, which

were closely related to morphological features, as discussed below.

2.4. Morphological Investigations

Surface and bulk morphologies were probed by atomic force microscopy (AFM) and AFM-based infrared spectroscopy (AFM-IR). All films exhibited smooth surfaces with small root-mean-square roughnesses of <1 nm (Figure S11, Supporting Information), which benefited the establishment of efficient ohmic contacts with the electron transport layer (PNDIT-F3N). Compared with the PM6:YSe film, the two DMA-based blend films exhibited more obvious fibrillar and successive phase separations (**Figure 5a**). As shown in Figure 5d and Figure S12 (Supporting Information), the calculated fibril diameters of the DYSe-1- and DYSe-2-based films are 22.5 ± 6 and 17.6 ± 7 nm, respectively, which were not only smaller than that of the PM6:YSe film (24.6 ± 6 nm) but also lied within the exciton diffusion distance (≈10–20 nm).[24] These distinct phenomena were further confirmed by AFM-IR (Figure 5b, blue and yellow colors represent PM6 and acceptor, respectively). The PM6:YSe film exhibited obvious acceptor-aggregation domains, which were significantly reduced in the PM6:DYSe-1 and PM6:DYSe-2 films. These results were consistent with AFM data. In particular, long-range connective acceptor domains with reduced diameters were observed in the PM6:DYSe-1 film. Broadly speaking, these distinctive morphological features of DMA-based films were associated with the suppressed charge recombination and charge transport therein.

GIWAXS measurements were performed to reveal the molecular stacking and crystallinity of the active layers. The preferred face-on molecular orientations of all acceptors were well maintained after blending with PM6, as supported by the notable (010) diffraction peak along the OOP direction and pronounced (100) lamellar diffraction peak along the IP direction (Figure 5c). In addition, as depicted in the 1D line cuts of the three blend films along the OOP direction (Figure 5e), a broad merged (010) peak was observed at similar positions (1.63–1.65 Å), which was mainly affected by PM6. The combined CLs of the films were estimated using the Scherrer equation, and the results show that the CL for PM6:YSe, PM6:DYSe-1, and PM6:DYSe-2 films were 16.6, 20.9, and 19.5 Å (Figure 5f; Table S7, Supporting Information), respectively. The largest CL and preferred face-on molecular orientations of the PM6:DYSe-1 film were more conducive to charge transport, in line with the best charge mobility properties of this film, resulting in the high J_{SC} and FF of the DYSe-1-based device. The above results suggest that the multiselenophene-substituted DMAs could decrease the self-aggregation of the monomer and thus form suitable fibrillar networks with improved CLs to provide a pathway for charge transportation, enabling efficient charge dynamics in blend films.

3. Conclusion

Two DMAs (DYSe-1 and DYSe-2) based on a typical selenophene-substituted SMA (YSe) were rationally designed and synthesized using the multiselenophene strategy. Compared with YSe, DYSe-1, and DYSe-2 exhibited more pronounced advantages of the selenophene unit and inherited broad absorption features extending to the near-infrared range (≈920 nm). In addition, the prepared DMAs were less susceptible to self-aggregation than YSe, which contributed to a more suitable and consecutive D/A phase separation in the PM6:DYSe-1 and PM6:DYSe-2 films. Hence, optimized charge dynamic properties were observed in the corresponding OSCs. As a result, DYSe-1- and DYSe-2-based OSCs achieved remarkable J_{SC} values of >27 mA cm^{-2}, ranking the best among the DMA-based binary devices reported to date. PM6:DYSe-1- and PM6:DYSe-2-based devices exhibited reduced E_{loss}, reasonably high V_{OC} (≈0.88 V), and excellent PCEs (>18%); moreover, this is the first report on multiselenophene-substituted DMA-based OSCs with PCEs above 18%. In addition, these devices displayed T_{80} lifetimes of >500 h under continuous thermal annealing, thereby showing satisfactory thermal stability. Our results not only demonstrate the successful application of the multiselenophene strategy to the construction of high-performance redshifted DMAs but also pave the way for the realization of high J_{SC} values and thus PCEs in DMA-based OSCs.

Supporting Information

Supporting Information is available from the Wiley Online Library or from the author.

Acknowledgements

The authors gratefully acknowledge the financial support from MoST of China (2022YFB4200400, 2019YFA0705900, and 2023YFE0210400), NSFC (52025033, 21935007, 52303237, and 22361132530). The authors thank Yu Chen at the Beijing Synchrotron Radiation Facility, Institute of High Energy Physics for performing GIWAXS measurements.

Conflict of Interest

The authors declare no conflict of interest.

Data Availability Statement

The data that support the findings of this study are available from the corresponding author upon reasonable request.

Keywords

dimeric acceptor, energy loss, multi-selenophene, organic solar cells, redshift

Received: February 29, 2024
Revised: April 23, 2024
Published online:

[1] a) L. Zhu, M. Zhang, J. Xu, C. Li, J. Yan, G. Zhou, W. Zhong, T. Hao, J. Song, X. Xue, Z. Zhou, R. Zeng, H. Zhu, C.-C. Chen, R. C. I. MacKenzie, Y. Zou, J. Nelson, Y. Zhang, Y. Sun, F. Liu, *Nat. Mater.* **2022**, *21*, 656; b) Y. Liu, B. Liu, C.-Q. Ma, F. Huang, G. Feng, H. Chen,

J. Hou, L. Yan, Q. Wei, Q. Luo, Q. Bao, W. Ma, W. Liu, W. Li, X. Wan, X. Hu, Y. Han, Y. Li, Y. Zhou, Y. Zou, Y. Chen, Y. Li, Y. Chen, Z. Tang, Z. Hu, Z.-G. Zhang, Z. Bo, *Sci China Chem* **2022**, *65*, 224; c) Y. Liu, B. Liu, C.-Q. Ma, F. Huang, G. Feng, H. Chen, J. Hou, L. Yan, Q. Wei, Q. Luo, Q. Bao, W. Ma, W. Liu, W. Li, X. Wan, X. Hu, Y. Han, Y. Li, Y. Zhou, Y. Zou, Y. Chen, Y. Liu, L. Meng, Y. Li, Y. Chen, Z. Tang, Z. Hu, Z.-G. Zhang, Z. Bo, *Sci China Chem* **2022**, *65*, 1457.

[2] J. Yi, G. Zhang, H. Yu, H. Yan, *Nat. Rev. Mater.* **2024**, *9*, 46.

[3] X. Wan, C. Li, M. Zhang, Y. Chen, *Chem. Soc. Rev.* **2020**, *49*, 2828.

[4] a) Y. Lin, J. Wang, Z.-G. Zhang, H. Bai, Y. Li, D. Zhu, X. Zhan, *Adv. Mater.* **2015**, *27*, 1170;. b) L. Zuo, S. B. Jo, Y. Li, Y. Meng, R. J. Stoddard, Y. Liu, F. Lin, X. Shi, F. Liu, H. W. Hillhouse, D. S. Ginger, H. Chen, A. K. Y. Jen, *Nat. Nanotechnol.* **2022**, *17*, 53.

[5] a) S. Chen, S. Zhu, L. Hong, W. Deng, Y. Zhang, Y. Fu, Z. Zhong, M. Dong, C. Liu, X. Lu, K. Zhang, F. Huang, *Angew. Chem., Int. Ed.* **2024**, *63*, e202318756; b) K. Liu, Y. Jiang, G. Ran, F. Liu, W. Zhang, X. Zhu, *Joule* **2024**, *8*, 835.

[6] a) Z. Zhong, S. Chen, J. Zhao, J. Xie, K. Zhang, T. Jia, C. Zhu, J. Jing, Y. Liang, L. Hong, S. Zhu, D. Ma, F. Huang, *Adv. Energy Mater.* **2023**, *13*, 2302273; b) Z. Chen, S. Zhang, T. Zhang, J. Ren, J. Dai, H. Li, J. Qiao, X. Hao, J. Hou, *Angew. Chem., Int. Ed.* **2024**, *63*, e202317892; c) L. Zhang, K. Yang, D. Qiu, J. Zhang, Z. Wei, K. Lu, *Chem. Eng. J.* **2024**, *481*, 148648.

[7] a) C. Yan, S. Barlow, Z. Wang, H. Yan, A. K. Y. Jen, S. R. Marder, X. Zhan, *Nat. Rev. Chem.* **2018**, *3*, 18003; b) J. Wang, P. Xue, Y. Jiang, Y. Huo, X. Zhan, *Nat. Rev. Chem.* **2022**, *6*, 614.

[8] a) C. Wang, X. Ma, Y.-f. Shen, D. Deng, H. Zhang, T. Wang, J. Zhang, J. Li, R. Wang, L. Zhang, Q. Cheng, Z. Zhang, H. Zhou, C. Tian, Z. Wei, *Joule* **2023**, *7*, 2386; b) J.-W. Lee, C. Sun, J. Lee, D. J. Kim, W. J. Kang, S. Lee, D. Kim, J. Park, T. N.-L. Phan, Z. Tan, F. S. Kim, J.-Y. Lee, X. Bao, T.-S. Kim, Y.-H. Kim, B. J. Kim, *Adv. Energy Mater.* **2024**, *14*, 2303872; c) Y. Gao, X. Yang, R. Sun, L.-Y. Xu, Z. Chen, M. Zhang, H. Zhu, J. Min, *Joule* **2023**, *7*, 2845.

[9] a) Z. Wang, X. Wang, L. Tu, H. Wang, M. Du, T. Dai, Q. Guo, Y. Shi, E. Zhou, *Angew. Chem., Int. Ed.* **2024**, *63*, e202319755; b) Z.-G. Zhang, Y. Li, *Angew. Chem., Int. Ed.* **2021**, *60*, 4422; c) Z.-G. Zhang, Y. Yang, J. Yao, L. Xue, S. Chen, X. Li, W. Morrison, C. Yang, Y. Li, *Angew. Chem., Int. Ed.* **2017**, *56*, 13503.

[10] a) J. Liu, W. Zhou, J. Deng, X. Geng, S. Y. Jeong, Y. Cui, H. Y. Woo, F. Wu, F. Liu, L. Chen, *Nano Energy* **2024**, *121*, 109218; b) X. Gu, X. Zhang, H. Huang, *Angew. Chem., Int. Ed.* **2023**, *62*, e202308496; c) C. Sun, J.-W. Lee, C. Lee, D. Lee, S. Cho, S.-K. Kwon, B. J. Kim, Y.-H. Kim, *Joule* **2023**, *7*, 416; d) M. Lv, Q. Wang, J. Zhang, Y. Wang, Z.-G. Zhang, T. Wang, H. Zhang, K. Lu, Z. Wei, D. Deng, *Adv. Mater.* **2024**, *36*, 2310046.

[11] a) P. Tan, H. Chen, H. Wang, X. Lai, Y. Zhu, X. Shen, M. Pu, H. Lai, S. Zhang, W. Ma, F. He, *Adv. Funct. Mater.* **2024**, *34*, 2305608; b) F. U. Rehman, S. Hameed, R. A. Khera, M. Shaban, M. Essid, Z. Aloui, S. I. Al-Saeedi, M. A. A. Ibrahim, M. Waqas, *ACS Omega* **2023**, *8*, 42492.

[12] a) X. Liu, Z. Zhang, C. Wang, C. Zhang, S. Liang, H. Fang, B. Wang, Z. Tang, C. Xiao, W. Li, *Angew. Chem., Int. Ed.* **2024**, *63*, e202316039; b) H. Chen, B. Kan, P. Wang, W. Feng, L. Li, S. Zhang, T. Chen, Y. Yang, T. Duan, Z. Yao, C. Li, X. Wan, Y. Chen, *Angew. Chem., Int. Ed.* **2023**, *62*, e202307962.

[13] F. Lin, K. Jiang, W. Kaminsky, Z. Zhu, A. K. Y. Jen, *J. Am. Chem. Soc.* **2020**, *142*, 15246.

[14] a) C. Yang, Q. An, M. Jiang, X. Ma, A. Mahmood, H. Zhang, X. Zhao, H.-F. Zhi, M. H. Jee, H. Y. Woo, X. Liao, D. Deng, Z. Wei, J.-L. Wang, *Angew. Chem., Int. Ed.* **2023**, *62*, e202313016; b) C. Yang, Q. An, H.-R. Bai, H.-F. Zhi, H. S. Ryu, A. Mahmood, X. Zhao, S. Zhang, H. Y. Woo, J.-L. Wang, *Angew. Chem., Int. Ed.* **2021**, *60*, 19241.

[15] a) G. Song, W. Feng, Y. Li, H. Liang, Z. Li, B. Kan, X. Wan, Z. Yao, C. Li, Y. Chen, *ChemComm.* **2023**, *59*, 10307; b) W. Gao, F. Qi, Z. Peng, F. R. Lin, K. Jiang, C. Zhong, W. Kaminsky, Z. Guan, C.-S. Lee, T. J. Marks, H. Ade, A. K.-Y. Jen, *Adv. Mater.* **2022**, *34*, 2202089.

[16] a) Z. Xia, J. Zhang, X. Gao, W. Song, J. Ge, L. Xie, X. Zhang, Z. Liu, Z. Ge, *ACS Appl. Mater.* **2021**, *13*, 23983; b) S. Liang, S. Li, Y. Zhang, T. Li, H. Zhou, F. Jin, C. Sheng, G. Ni, J. Yuan, W. Ma, H. Zhao, *Adv. Funct. Mater.* **2021**, *31*, 2102764.

[17] H. Chen, T. Zhao, L. Li, P. Tan, H. Lai, Y. Zhu, X. Lai, L. Han, N. Zheng, L. Guo, F. He, *Adv. Mater.* **2021**, *33*, 2102778.

[18] H. Chen, Z. Zhang, P. Wang, Y. Zhang, K. Ma, Y. Lin, T. Duan, T. He, Z. Ma, G. Long, C. Li, B. Kan, Z. Yao, X. Wan, Y. Chen, *Energy Environ. Sci.* **2023**, *16*, 1773.

[19] Y. Shi, Y. Chang, K. Lu, Z. Chen, J. Zhang, Y. Yan, D. Qiu, Y. Liu, M. A. Adil, W. Ma, X. Hao, L. Zhu, Z. Wei, *Nat. Commun.* **2022**, *13*, 3256.

[20] a) L. Zhu, J. Zhang, Y. Guo, C. Yang, Y. Yi, Z. Wei, *Angew. Chem., Int. Ed.* **2021**, *60*, 15348; b) X. Li, Y. Wu, S. Zhang, B. Cai, Y. Gu, J. Song, H. Zeng, *Adv. Funct. Mater.* **2016**, *26*, 2435.

[21] a) J. Shi, Z. Chen, H. Liu, Y. Qiu, S. Yang, W. Song, Z. Ge, *Adv. Energy Mater.* **2023**, *13*, 2301292; b) J. Zhang, S. Luo, H. Zhao, X. Xu, X. Zou, A. Shang, J. Liang, F. Bai, Y. Chen, K. S. Wong, Z. Ma, W. Ma, H. Hu, Y. Chen, H. Yan, *Angew. Chem., Int. Ed.* **2022**, *61*, e202206930.

[22] a) F. Liu, Y. Jiang, R. Xu, W. Su, S. Wang, Y. Zhang, K. Liu, S. Xu, W. Zhang, Y. Yi, W. Ma, X. Zhu, *Angew. Chem., Int. Ed.* **2024**, *63*, e202313791; b) H. Lu, W. Liu, G. Ran, Z. Liang, H. Li, N. Wei, H. Wu, Z. Ma, Y. Liu, W. Zhang, X. Xu, Z. Bo, *Angew. Chem., Int. Ed.* **2023**, *62*, e202314420; c) Z. Gan, L. Wang, J. Cai, C. Guo, C. Chen, D. Li, Y. Fu, B. Zhou, Y. Sun, C. Liu, J. Zhou, D. Liu, W. Li, T. Wang, *Nat. Commun.* **2023**, *14*, 6297;. d) Z. Li, Z. Zhang, H. Chen, Y. Zhang, Y.-Q.-Q. Yi, Z. Liang, B. Zhao, M. Li, C. Li, Z. Yao, X. Wan, B. Kan, Y. Chen, *Adv. Energy Mater.* **2023**, *13*, 2300301; e) J. Wu, Z. Ling, L. R. Franco, S. Y. Jeong, Z. Genene, J. Mena, S. Chen, C. Chen, C. M. Araujo, C. F. N. Marchiori, J. Kimpel, X. Chang, F. H. Isikgor, Q. Chen, H. Faber, Y. Han, F. Laquai, M. Zhang, H. Y. Woo, D. Yu, T. D. Anthopoulos, E. Wang, *Angew. Chem., Int. Ed.* **2023**, *62*, e202302888; f) J. Wan, T. Wang, R. Sun, X. Wu, S. Wang, M. Zhang, J. Min, *Adv. Mater.* **2023**, *35*, 2302592.

[23] a) Q. Fan, R. Ma, J. Yang, J. Gao, H. Bai, W. Su, Z. Liang, Y. Wu, L. Tang, Y. Li, Q. Wu, K. Wang, L. Yan, R. Zhang, F. Gao, G. Li, W. Ma, *Angew. Chem., Int. Ed.* **2023**, *62*, e202308307; b) Z. Li, X. Li, J. Xue, J. Zhang, C. Zhu, J. Li, W. Ma, L. Meng, Y. Li, *ACS Energy Lett.* **2023**, *8*, 2488; c) Y. Li, Z. Chen, X. Yan, Z. Ge, *Carbon Energy* **2023**, *6*, e439.

[24] a) Z. Fu, J.-W. Qiao, F.-Z. Cui, W.-Q. Zhang, L.-H. Wang, P. Lu, H. Yin, X.-Y. Du, W. Qin, X.-T. Hao, *Adv. Mater.* **2024**, 2313532; b) F. Sun, X. Zheng, T. Hu, J. Wu, M. Wan, Y. Xiao, T. Cong, Y. Li, B. Xiao, J. Shan, E. Wang, X. Wang, R. Yang, *Energy Environ. Sci.* **2024**, *17*, 1916; c) J. Zhang, B. Kan, A. J. Pearson, A. J. Parnell, J. F. K. Cooper, X.-K. Liu, P. J. Conaghan, T. R. Hopper, Y. Wu, X. Wan, F. Gao, N. C. Greenham, A. A. Bakulin, Y. Chen, R. H. Friend, *J. Mater. Chem. A* **2018**, *6*, 21618.